Lasers in Manufacturing Conference 2015

# Evaluation of picosecond laser-induced shunt resistance in CIGS thin-film solar cells

Edgaras Markauskas*, Paulius Gečys, Gediminas Račiukaitis

*Center for Physical Sciences and Technology, Savanoriu Ave. 231, Vilnius, LT-02300, Lithuania*

**Abstract**

CIGS thin films became even more attractive to PV industry after rapid efficiency increase over the last years for small scale devices. However, the transition from the small scale to full-sized modules introduces efficiency losses due to increased photocurrent and related ohmic losses. On the other hand, the high efficiency can be maintained if the large module area is divided into many smaller segments interconnected in series by a three-step patterning process. We utilized a picosecond laser working at the 532 nm wavelength to perform P3 type scribing process to separate the adjacent cells. Initially, we applied the technique of nested circular scribes proposed by K. Zimmer to evaluate the laser-induced shunt resistance after the P3 process. Further, we investigated the model including the top-contact resistance effects to the I-V measurement. Finally, we applied a simpler laser-induced shunt evaluation model by performing the P3 scribes between screen-printed silver grids of the CIGS mini cells. In both cases, parallel resistance values of the cells were extracted by analyzing I-V characteristics. Both evaluation techniques allowed to improve the laser parameter optimization process and the measurement accuracy of shunt formation during the laser scribing.

Keywords: CIGS, laser scribing, P3, parallel conductivity,

## 1. Introduction

CIGS ($CuIn_xGa_{(1-x)}Se_2$) absorber based solar cells holds the leader position in the conversion of sunlight energy into electricity as the most efficient amongst the thin-film competitors. Despite this, manufacturers seem to find ways to increase further the efficiency, and recently ZSW (Germany) announced a new CIGS mini-cell record of 21.7 % (Jackson, P. et al., 2015). However, the full-sized CIGS modules fabricated under

* Corresponding author. Tel.: +370 682 50083.
*E-mail address:* edgaras.markauskas@ftmc.lt

industrial conditions suffer significant efficiency drop (Powalla, M. et al., 2003). Losses arise due to the thin resistive transparent electrodes and contacts. Since the magnitude of generated photocurrent is proportional to the active cell area, the high conversion efficiency can be maintained by dividing large module area into smaller cells and interconnecting them in series. In that way, photocurrent, and hence resistance losses are reduced which are crucial for the performance of the device (Gecys, P. et al., 2013).

The most common patterning method consists of three scribing processes identified as P1, P2 and P3. Integration of a laser tool is very promising. However, it is still facing many unsolved challenges, one of which is material modification at the scribing area (Wang, X. et al., 2013). It may result in a formation of electro-conductive secondary phases (Romero, E. et al., 2006). Consequently, reliable methods must be applied to evaluate the variation of parallel conductance and further optimize the laser process.

In this paper, we concentrated on the specific P3 isolation scribe by removing the transparent front conductive oxide (TCO) and leaving the CIGS absorber undamaged. This method already proved to be as sufficient as "classical" P3 scribe, which involves the removal of both TCO and CIGS layers (Burn, A. et al., 2013).

We applied the nested circular laser scribing (NCLST) (Wang, X. et al., 2013) and the linear laser scribing (LLST) techniques to evaluate laser-induced parallel conduction variation after the isolating P3 scribe.

## 2. Experimental

### *2.1. Samples*

We conducted our experiments on two types of complete CIGS solar cells. Initially, the NCLST technique was applied to a complete cell which consisted of the ZnO:Al top-contact (350 nm), CdS buffer layer (50 nm), CIGS active layer (2 µm) and 500 nm thick molybdenum (Mo) back-contact. The LLST technique was applied to the second CIGS cell consisting of 500 nm TCO, 50 nm CdS, 1.3 µm CIGS and 500 nm thick Mo layer. Both structures were deposited on polyimide (PI) substrates.

### *2.2. Laser source*

Laser scribing experiments were carried out using a diode-pumped Nd:$YVO_4$ ultra-short pulse laser operating at the second harmonics (532 nm radiation wavelength) with a pulse duration of 10 ps at 50 – 500 kHz repetition rate. The setup included 80 mm f-theta lens and galvanometer scanner (from ScanLab), as well as, polarization based attenuator system.

### *2.3. Nested circular and linear laser scribing techniques*

The nested circular laser scribing technique (NCLST) was recently proposed by K. Zimmer group [4]. The technique consists of concentric circular laser scribes performed on the solar cell's front surface. Starting from the outermost circular scribe, every consecutive scribe must be carried out with a radius slightly decreased. In between the scribes, the solar cell's parallel conductance is measured. Eventually, every measured value is plotted versus the corresponding radius of the scribed circle and fitted with the proposed fitting function. Fitting function and more detailed information on the model can be found in [4]. However, the approach has a wider applicability since solar cell areal and defect conductance values can be extracted as well.

A more straightforward approach to evaluating laser-induced parallel conductance is based on the scribing of straight multiple laser trenches. As in the NCLST case, the parallel conductance measurements

are performed after every single scribe, plotted against corresponding scribe length, and finally fitted with a simple linear function. The fitting function's slope indicates the laser-induced parallel conductance.

For the on-line parallel conductance measurements, we used the 4 point I-V measurement system Keithley 2602A.

## 3. Results

### *3.1. NCLST results using 532 nm radiation wavelength*

To fulfill the demands for the high P3 process yield, the laser scribing speed was set to 800 mm/s combined with 15 µJ energy pulses. Laser irradiation wavelength was 532 nm. Defocused laser beam affected the width of the trench that was measured to be 55 µm. SEM image of the scribe is shown in figure 1. The radius of the outermost circle was 10 mm. Every other circle was scribed with a radius smaller by 200 µm. Due to the contact shading, the radius of the smallest circle was limited to 8 mm.

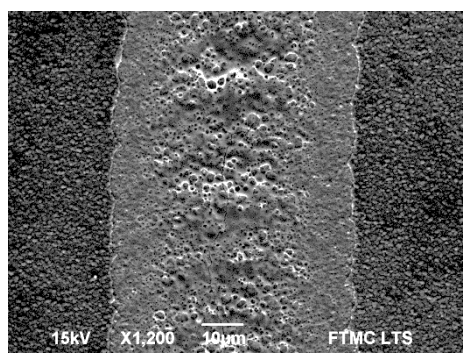


Fig. 1. Scanning electron microscope image of scribed P3 trench in CIGS solar cell.

Several experiments using identical laser parameters were conducted. Two of those experiments are presented in Fig. 2a and 2b. Here, the experimentally measured cell's parallel conductance is presented as square dots while fitting results are shown as continuous black curves. Sudden drops in the parallel conductivity are caused by the isolation of prior defects in CIGS material. The technique showed good results reported in (Wang, X. et al., 2013). However, in our case, the model was inaccurate since extracted areal conductance values were scattered, and in some cases even were negative (experiment No. 1 $\sigma_{SCA}$ = -21.8 S/m$^2$). However, the laser-induced conductance values $\sigma_{SCM}$ were of the same order of magnitude: 9.9 S/m and 6.7 S/m for first and second experiments, respectively (see Table 1). The reason for the model inaccuracy may rise because the effect of the serial resistance $R_s$ of TCO was neglected. It was considered that the layer resistance was negligible compared to the device parallel resistance. Hence, it would not affect measurement results. However, in our case the CIGS layer conductivity was much higher compared to values reported in (Wang, X. et al., 2013) and could influence the results.

Table 1. Extracted conductance values from the fitting function.

| | Experiment No. 1 | Experiment No. 2 |
|---|---|---|
| Areal conductance, S/m$^2$ | -21.7 | 98.1 |
| Laser-induced conductance, S/m | 9.9 | 6.7 |

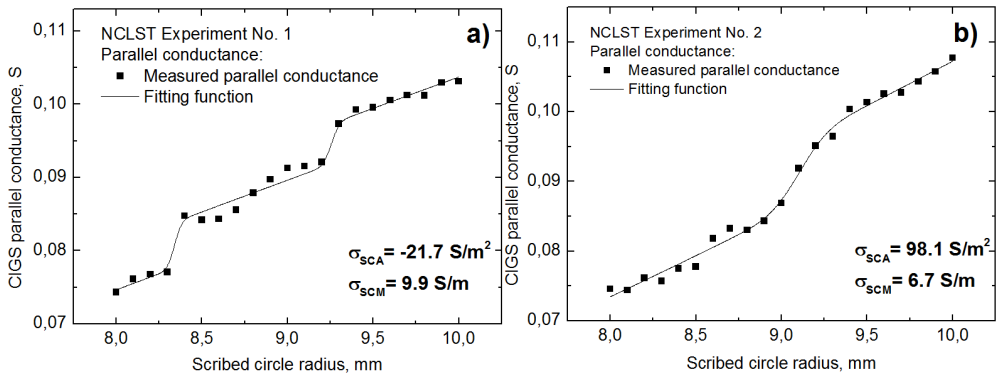


Fig. 2. Solar cell's parallel conductance dependence on the scribed circle radius. Graphs (a) and (b) depicts two separate NCLST experiments carried out using the identical scribing parameters.

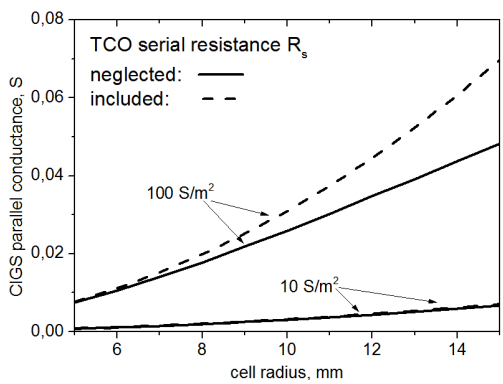


Fig. 3. Simulation of CIGS mini-cell parallel conductivity dependence on the radius of the cylindrical structure. Low (10 S/m$^2$) and high (100 S/m$^2$) CIGS cell areal conductivity cases simulated.

To investigate the TCO serial resistance effects to the solar cell's parallel conductance measurement, we conducted a simple model that was implemented into Comsol Multiphysics$^{tm}$ environment. The model was solved following the Ohm's law, and simulation was selected to be 2D axis-symmetric in order to match NCLST experiment geometry. While CdS, Mo and TCO layer characteristics were constant, we varied CIGS conductivity to match the experimental results. The modeled parallel conductance versus the solar cell radius is plotted in figure 3. The dashed line represents the ideal case where the TCO serial resistance is completely neglected. Continuous curve stands for the small-area contact positioned in the middle of the modeled structure taking into account the top-contact resistivity. The difference between the ideal case and the TCO resistance effects could evoke significant measurement errors. These errors tend to grow with the increasing CIGS conductivity (see figure 3). In contrast, it can be seen that the measurement errors for the 10 S/m$^2$ sample should be negligible. The resultant error was likely responsible for the obtained inaccurate results.

Modeling described above can be applied to the LLST technique as well. The scribe radius can be interpreted as a distance between the scribe and the I-V probe. For the 10 S/m$^2$ parallel conductance samples, the distance between the scribe and position of the I-V probes may exceed several centimetres

with the errors still insignificant. In the case of 100 S/m$^2$ samples, the “secure” scribe distance would be considerably lower.

### *3.2. LLST results using 532 nm radiation wavelength*

In the second part of our experiments, we applied the linear laser scribing technique (LLST). We performed eleven 1.8 cm-long P3 scribes in a CIGS sample. Scribes were positioned parallel to the screen-printed silver grids, and the parallel conductivity measurements were applied after each scribe. The scribe distance to the nearest grid did not exceed 1.5 mm. Laser parameters similar to that used in the NCLST experiments were applied.

Measured CIGS cell’s parallel conductivity versus the length of the scribed trench is plotted in figure 4. Extracted laser-induced conductance was equal to $\sigma_{SCM}$ = 0.016 S/m. Obtained value is in close agreement with the results achieved in CIGS cells reported by the authors of the NCLST technique (Wang, X. et al., 2013). The effect of the TCO serial resistance was negligible in this case, since a linear dependence of the CIGS parallel resistance on the scribe length was observed. The LLST approach allows to localize tightly, and position laser performed scribes near the measuring probes and makes it possible to avoid measuring errors caused by the finite conductance of the TCO layer.

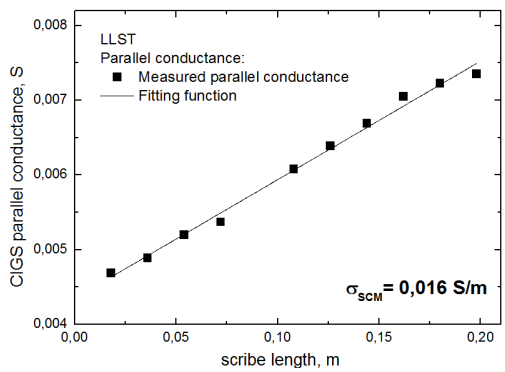


Fig. 4. . Solar cell’s parallel conductivity dependence on scribed trench length. Linear laser scribing technique (LLST) was applied.

## 4. Conclusions

We applied two similar approaches to evaluating the laser-scribe specific conductivity. The nested circular laser scribing technique showed inaccurate results for the CIGS samples with the parallel conductance higher than 98 S/m.

Modeling revealed crucial importance to preselect the correct scribing distance to the I-V measuring probes for cells with a parallel conductance of 100 S/m$^2$ and more. In the case of the 10 S/m$^2$ CIGS samples, the measurement errors resulting from small area I-V probes can be neglected.

The linear laser scribing technique (LLST) is more straightforward and allows optimization of the scribing geometry that can lower the TCO serial resistance effects. If solar cell’s areal conductance or conductance of localized defects is not a purpose of the measurements, the LLST technique would be a simpler and faster approach.

## Acknowledgements

The research leading to these results was partially funded by the European Union FP7 Programme under grant agreement No 609355 (APPOLO). We acknowledge our thanks to Solarion AG, Germany, for kind support with the samples.

## References

Jackson, P., Hariskos, D., Wuerz, R., Kiowski, O., Bauer, A., Friedlmeier, T. M.,Powalla, M., 2015. Properties of Cu(in,Ga)Se2 Solar Cells with New Record Efficiencies up to 21.7%, physica status solidi (RRL) – Rapid Research Letters 9, p. 28-31.

Powalla, M., Hariskos, D., Lotter, E., Oertel, M., Springer, J., Stellbogen, D., Dimmler, B.,Schäffler, R., 2003. Large-Area Cigs Modules: Processes and Properties, Thin Solid Films 431–432, p. 523-533.

Gecys, P., Markauskas, E., Raciukaitis, G., Repins, I.,Beall, C., 2013. Selective Front Side Patterning of CZTS Thin-Film Solar Cells by Picosecond Laser Induced Material Lift-Off Process, Phys. Procedia 41, p. 734-738.

Wang, X., Ehrhardt, M., Lorenz, P., Scheit, C., Ragnow, S., Ni, X. W.,Zimmer, K., 2013. In-Process Measuring of the Electrical Shunt Resistance of Laser-Scribed Thin-Film Stacks by Nested Circular Scribes, Review of Scientific Instruments 84.

Romero, E., Calderón, C., Bartolo-Pérez, P., Mesa, F.,Gordillo, G., 2006. Phase Identification and Aes Depth Profile Analysis of Cu(in,Ga)Se2 Thin Films, Brazilian Journal of Physics 36, p. 1050-1053.

Burn, A., Muralt, M., Pilz, S., Romano, V., Witte, R., Frei, B., Buecheler, S., Nishiwaki, S.,Krainer, L., 2013. All Fiber Laser Scribing of Cu(in,Ga)Se2 Thin-Film Solar Modules, Phys. Procedia 41, p. 713-722.